Supporting Information for: Nanoscopic Approach to Quantification of Equilibrium and Rate Constants of Complex Formation at Single-Molecule Level

Xuzhu Zhang,[†] Evangelos Sisamakis,[‡] Krzysztof Sozanski,[†] and Robert Holyst[*,†]

[†]*Department of Soft Condensed Matter, Institute of Physical Chemistry, Polish Academy of Sciences, Warsaw, Poland*

[‡]*PicoQuant GmbH, Berlin, Germany*

E-mail: rholyst@ichf.edu.pl

S1 Experimental details

Both excitation and depletion lasers (LDH-640 and VisIR 765 "STED") were operated in pulsed mode.[1] The repetition rate of the excitation laser was 40 MHz (i.e., one pulse every 25 ns), while the STED laser was operated at half of this frequency. Therefore, STED pulse was introduced after every other excitation pulse, so that an intrinsic, on-line non-STED reference was recorded for each measurement (cf. upper panel of Fig. S1). Each recorded photon was assigned either to the excitation-only or excitation-with-STED pulse.

In the STED section of the histogram, the fluorescence decay had another fast component, which mostly originated from the bleed-through of the stimulated emission to the detection channel. Because these photons were from the depleted region (outside the intended observation volume), we disregarded them and only included in the autocorrelation photons recorded between 2.6 and 25 ns (patterned area in the upper panel of Fig. S1) to increase the resolution and data quality of STED-FCS.[2–4] Since the delay between pulses was at least three orders of magnitude shorter than the diffusion time, the pulsed mode operation did not influence the autocorrelation in the range of diffusion-related lag times.

The fluorescence intensity of ATTO647N under STED condition (I_{STED}) was gradually reduced as the increasing of STED power, comparing to its non-STED reference (I_{FCS}) in the same measurement (see the lower panel of Fig. S1). The saturation power of ATTO647N, P_{SAT}, was determined by finding the value of P_{STED} at which the fluorescence intensity dropped by half according to the definition of P_{SAT}. The determined saturation power for ATTO647N was 11 mW.

In addition to STED-FCS, non-super-resolution FCS measurements (Section S4 were performed on a Nikon A1 confocal microscope with a 60× /1.27 water immersion objective (Nikon Plan Apo). The system was equipped with PicoQuant upgrade kit comprising MPD SPAD detectors and PicoHarp 300 TCSPC module. For excitation of ATTO647N and Alexa647, a 643 nm diode laser was used (Melles Griot, 56RCS series, constant wave). SymPhoTime 64 software and gnuplot (version 4.5) were used for data analysis.

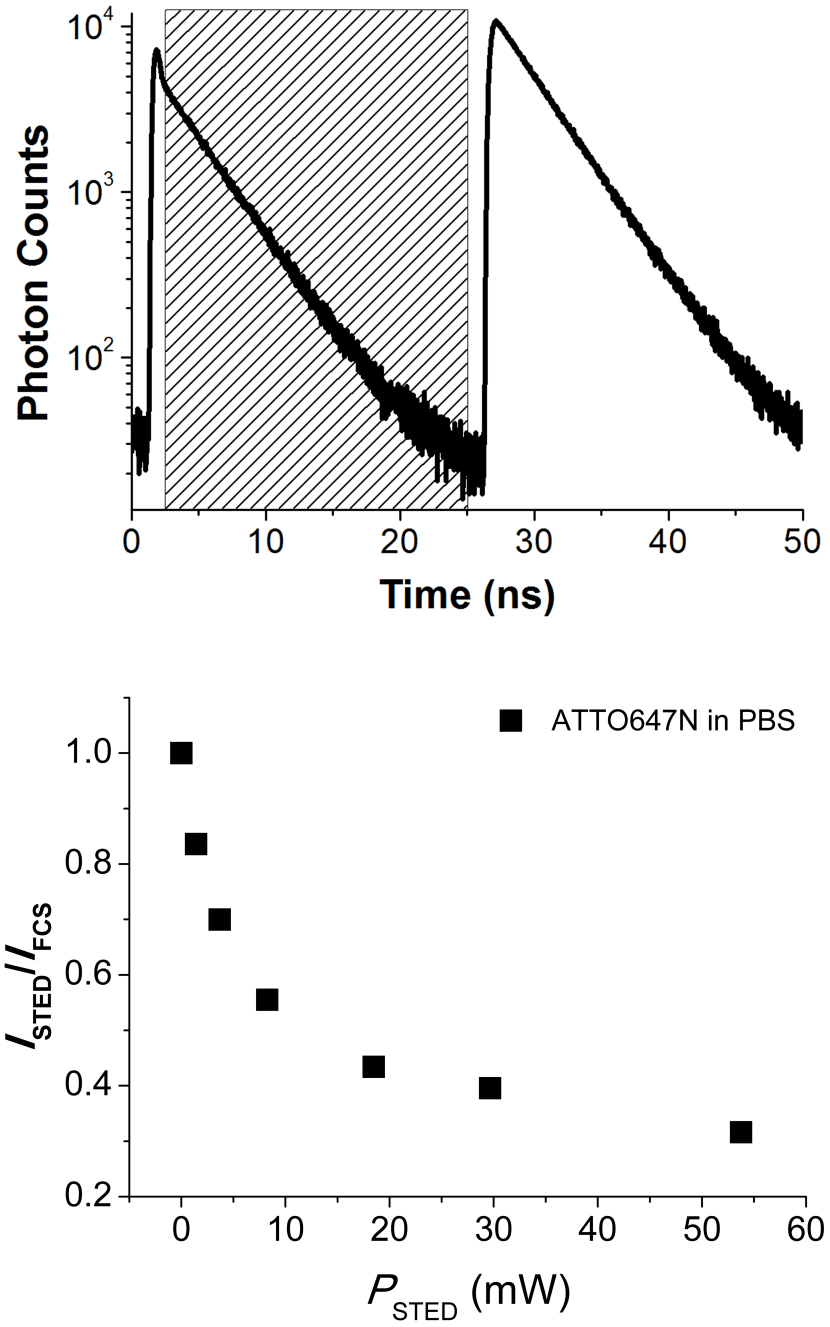

Figure S1: Upper panel: representative TCSPC histogram recorded during a STED-FCS measurement ($P_{\mathrm{STED}}/P_{\mathrm{SAT}} = 1.7$) of ATTO647N in PBS. STED pulse was introduced only in the first part (1.7−2.2 ns) synchronizing with the excitation pulse, while in the second part of the cycle only excitation pulse was applied (from 26.7 ns). Photons were assigned to the STED and non-STED sections using time-tagging. Thus, an intrinsic non-STED reference was recorded within every measurement. Lower panel: The ratio of fluorescence intensity of ATTO647N under the STED condition, I_{STED}, to the non-STED condition, I_{FCS}, as a function of STED power P_{STED}. The $P_{\mathrm{SAT}} = 11$ mW was determined by finding the value of P_{STED} where $I_{\mathrm{STED}}/I_{\mathrm{FCS}} = 0.5$.

S2 Autocorrelation model for diffusion-reaction systems

The molecular interaction between component A and B can be treated as binary reaction:[5,6]

$$\mathrm{A} + \mathrm{B} \underset{}{\overset{K}{\rightleftharpoons}} \mathrm{C}$$

where C stands for complexes. The equilibrium constant K is related to the association and dissociation rate constants (k_+, k_-) and the concentrations of each component at the equilibrium state ($[A]^{\mathrm{eq}}$, $[B]^{\mathrm{eq}}$, $[C]^{\mathrm{eq}}$) as $K = k_+/k_- = [C]^{\mathrm{eq}}/[A]^{\mathrm{eq}}[B]^{\mathrm{eq}}$. The relaxation rate R of the interaction, which describes the rate of the reaction returning to the equilibrium, is defined as $R = k_+([A]^{\mathrm{eq}} + [B]^{\mathrm{eq}}) + k_-$.[6]

Derivation of the model for diffusion-reaction systems is based on the framework of Magde's theory and our previous work.[5–7] In our dye-micelle systems we assume that the size of micelles is roughly uniform (within the concentration range investigated) and much larger than that of the dyes, so the diffusion coefficient of micelles is not affected by attachment of a dye molecule, namely $D_{\mathrm{A}} = D_{\mathrm{C}} \gg D_{\mathrm{B}}$. The quantum yield of the dye does not change significantly after binding to the micelle. The full expression for was presented in our previous paper,[7] here we show the simplified form as:

$$\begin{aligned} G_{\mathrm{a}}(\tau) = \; & G(0)\Bigg\{ (1+\tau_+)^{-1}\left(1+\tau/\left(\kappa^2\tau_+\right)\right)^{-1/2}\left[1-\exp\left(-R\tau_\Delta(1+\frac{\tau}{\tau_+})\right)\right] \\ & + \beta\,(1+\tau_{\mathrm{A}})^{-1}\left(1+\tau/\left(\kappa^2\tau_{\mathrm{A}}\right)\right)^{-1/2}\exp\left(-R\tau_\Delta(1+\frac{\tau}{\tau_+})\right) + \\ & (1-\beta)\,(1+\tau_{\mathrm{B}})^{-1}\left(1+\tau/\left(\kappa^2\tau_{\mathrm{B}}\right)\right)^{-1/2}\exp\left(-R\tau\right)\exp\left(-R\tau_\Delta(1+\frac{\tau}{\tau_-})\right)\Bigg\}, \end{aligned} \tag{S1}$$

where $\tau_\pm = \omega^2/4D_\pm$, $\tau_\Delta = \omega^2/4D_\Delta$, $\tau_{\mathrm{A}} = \omega^2/4D_{\mathrm{A}}$, $\tau_{\mathrm{B}} = \omega^2/4D_{\mathrm{B}}$ are the effective diffusion times within the observation volume of a radius ω. The corresponding effective diffusion coefficients $D_+ = D_{\mathrm{A}}\beta + D_{\mathrm{B}}(1-\beta)$, $D_- = D_{\mathrm{A}}(1-\beta) + D_{\mathrm{B}}\beta$, $\Delta = D_{\mathrm{A}} - D_{\mathrm{B}}$, where $\beta = k_+[A]^{\mathrm{eq}}/R = K[A]^{\mathrm{eq}}/(1+K[A]^{\mathrm{eq}})$. κ is the structure parameter (describing the axial elongation of the observation volume) known from calibration. The model features only one free parameter (R) which needs to be fitted, while the rest of the parameters ($\tau_\pm, \tau_\Delta$, and

β), whose values depend on the size of observation volume, equilibrium constant and the micelle concentration, can be exactly fixed during the fitting procedure.

In case of dyes diffusing in relatively concentrated solutions of micelles (large value of R) within a large observation volume (large value of τ_Δ), the value of $R\tau_\Delta \to \infty$ according to the definition of both quantities. Then, Eq. S1 reduces to the known form for the single-component diffusion:

$$G_\infty(\tau) = G(0)(1+\tau/\tau_+)^{-1}\left(1+\tau/\left(\kappa^2\tau_+\right)\right)^{-1/2}, \tag{S2}$$

whereby only a single value of the effective diffusion time can be obtained from autocorrelation fitting. This expression is equivalent to the typical single-component model for FCS (see Eq. 4 in the main text).

For dyes diffusing in the dilute solutions of micelles (small value of R) within small observation volumes (small value of τ_Δ), $R\tau_\Delta \to 0$ and Eq. S1 reduces to

$$G_0(\tau) = G(0)\left[\beta\left(1+\tau/\tau_{\mathrm{A}}\right)^{-1}\left(1+\tau/\left(\kappa^2\tau_{\mathrm{A}}\right)\right)^{-1/2} + (1-\beta)\left(1+\tau/\tau_{\mathrm{B}}\right)^{-1}\left(1+\tau/\left(\kappa^2\tau_{\mathrm{B}}\right)\right)^{-1/2}\right], \tag{S3}$$

This expression is equivalent to the standard two-component model for FCS,[8] where β represents the fraction of complexes in the system.

S3 Observation volume profile in STED-FCS

We describe the profile of the depleting beam, $p_{\mathrm{STED}}(\mathbf{r})$ visualized in middle panel of Fig. S2, as:[9]

$$p_{\mathrm{STED}}(\mathbf{r}) = \frac{1}{\sqrt{1+z/z_{\mathrm{R}}}}\left(\frac{r}{\omega_{\mathrm{STED}}(z)}\right)^2 \exp\left(\frac{-2r^2}{\omega^2_{\mathrm{STED}}(z)}\right) \tag{S4}$$

where z_{R} is the Rayleigh length expressed as $z_{\mathrm{R}} = \pi\omega_0^2/\lambda$ and ω_0 is the STED beam waist. To obtain the effective detection profile $p_{\mathrm{eff}}(\mathbf{r})$ we need to overlay the confocal detection profile

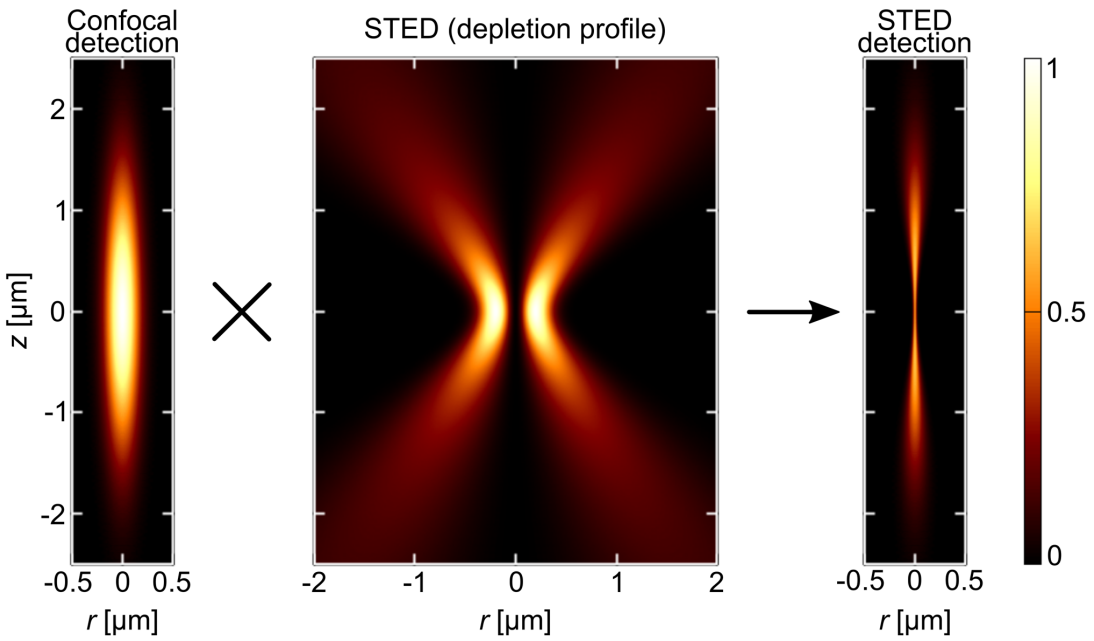

Figure S2: Calculated detection profiles for the STED-FCS setup used in this study (excitation wavelength: 640 nm, beam waist: 230 nm, confocal aspect ratio: 8). Left: confocal detection profile $p_{\mathrm{conf}}(\mathbf{r})$; middle: STED depletion profile $p_{\mathrm{STED}}(\mathbf{r})$; right: effective detection profile $p_{\mathrm{eff}}(\mathbf{r})$. The detection and depletion profiles are independently normalized to exhibit value of 1 at the brightest point.

in 3D Gaussian distribution $p_{\mathrm{conf}}(\mathbf{r}) = \exp(-2r/\omega_{\mathrm{conf}}^2)\exp(-2z/z_{\mathrm{conf}}^2)$ with the depleting beam profile p_{STED}, including the non-linear dependence of depletion efficiency on STED intensity:[10]

$$p_{\mathrm{eff}}(\mathbf{r}) = p_{\mathrm{conf}} \exp(-a p_{\mathrm{STED}}) \tag{S5}$$

where a is a dimensionless parameter defining the total STED intensity. The total spontaneous fluorescence intensity corresponds to the integral of $p_{\mathrm{eff}}(\mathbf{r})$ over the whole space. For any given z position, $p_{\mathrm{eff}}(\mathbf{r})$ maintains a Gaussian distribution. However, the width of this Gaussian is a function of z and $p_{\mathrm{eff}}(z)$ is not Gaussian (see Fig. S2).

Obviously the focal plane of observation volume created by the excitation beam is the most effectively depleted while the axial section is relatively elongated. Additionally, due to the lack of pinhole for the STED beam, the shape of observation volume becomes broader and dimmer along the axial direction. As a consequence, the fluorescences originating from

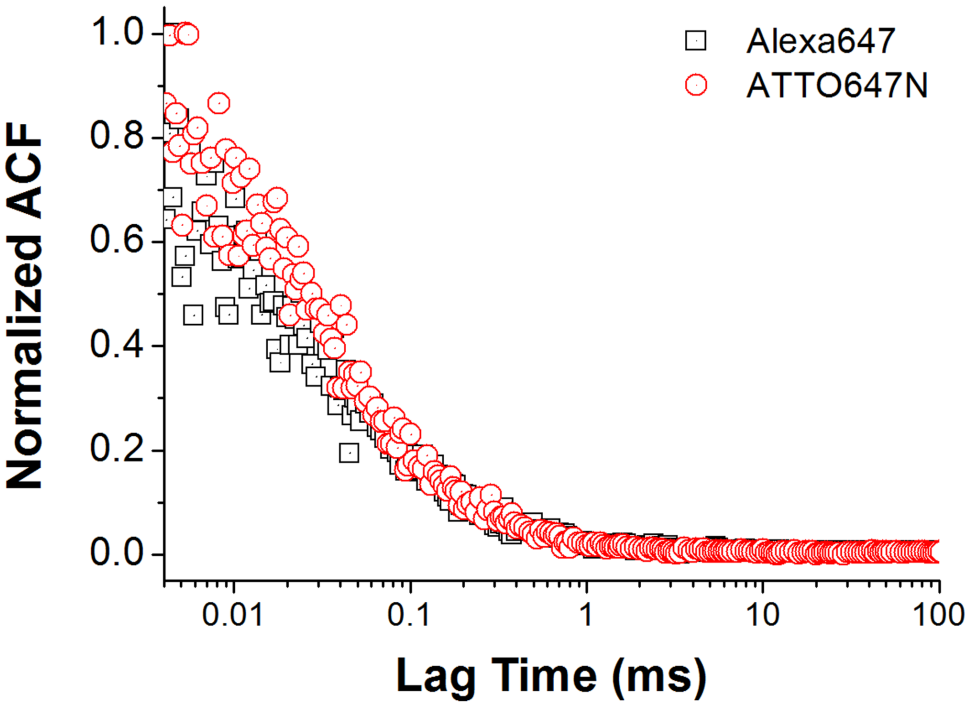

Figure S3: Experimental autocorrelation curves (ACFs) of ATTO647N and Alexa647 diffusing in water using FCS.

these dim fringes are more likely to be recognized as background noise rather than signals. The axial diffusion of the probes contribute to the autocorrelation function negligibly. These factors justify application of a simple 2D autocorrelation fitting model.[9]

S4 Diffusion coefficient of ATTO647N

Diffusion coefficient of ATTO647N in water, D_{atto}, was determined by FCS based on the calibration measurements of another dye Alexa647 (purchased from Sigma), whose diffusion coefficient D_{alexa} in water at 298 K is known to be 330 $\mu\text{m}^2\text{s}^{-1}$ from the literature.[11] The value of $D_{\text{atto}} = 352\ \mu\text{m}^2\text{s}^{-1}$, was determined from the relation $D_{\text{atto}} = D_{\text{alexa}}\tau_{\text{atto}}/\tau_{\text{alexa}}$, where τ_{atto} and τ_{alexa} were the fitted diffusion times of the respective dye in the FCS observation volume. Single-component model (Eq. S2) was used for ACF fitting.

S5 Test of the two-component model in the large observation volume regime

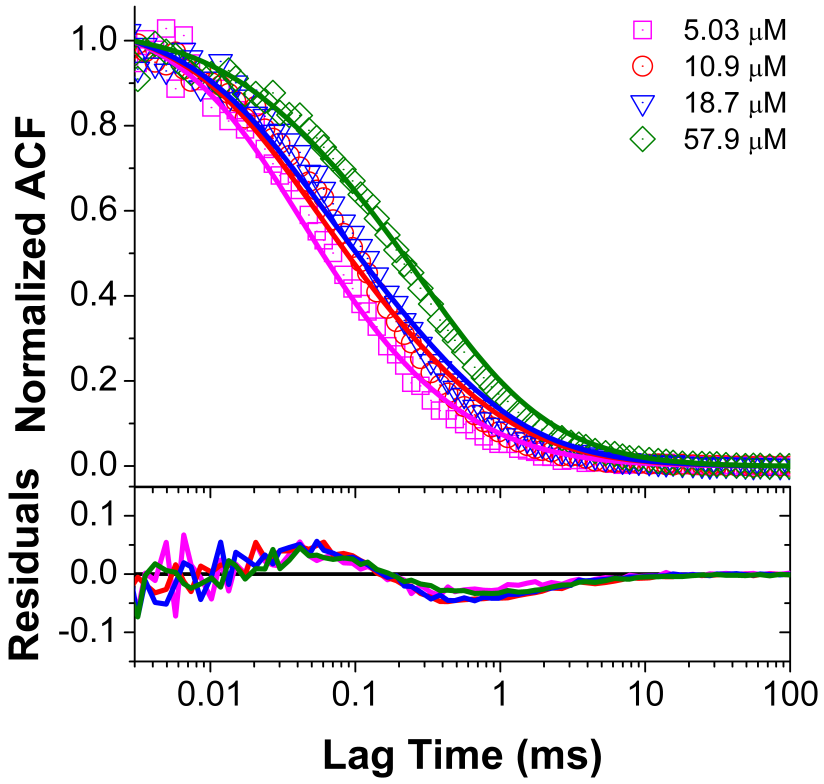

Figure S4: Experimental autocorrelation curves of ATTO647N in the $C_{12}E_8$ solutions (open symbols) and corresponding fits of the 3D, two-component model (Eq. S3, solid lines). Apparently, the fits were too poor to rely on due to the large residuals.

We attempted to fit the recorded autocorrelation curves of ATTO647N diffusing in $C_{12}E_8$ solutions with the two-component model for 3D systems (cf. Eq. S3). The parameters concerning the diffusion times of dyes and micelles within the observation volume (τ_A and τ_B) were fixed on the basis of calibration data, however, the fits were too poor to rely on according to the residuals (see Fig. S4). Therefore, we concluded that it was not appropriate to apply the two-component model for the analysis of the ACFs within this concentration range. This is in line with our predictions regarding the various regimes defined by the ratio of relaxation

rate to diffusion time. In the large observation volume, fast association/dissociation processes affect the signal at the time-scale of observation and the full reaction-diffusion model (see Section S2) is required for quantitative data analysis.

S6 ATTO647N in $C_{12}E_8$ solutions under various STED powers

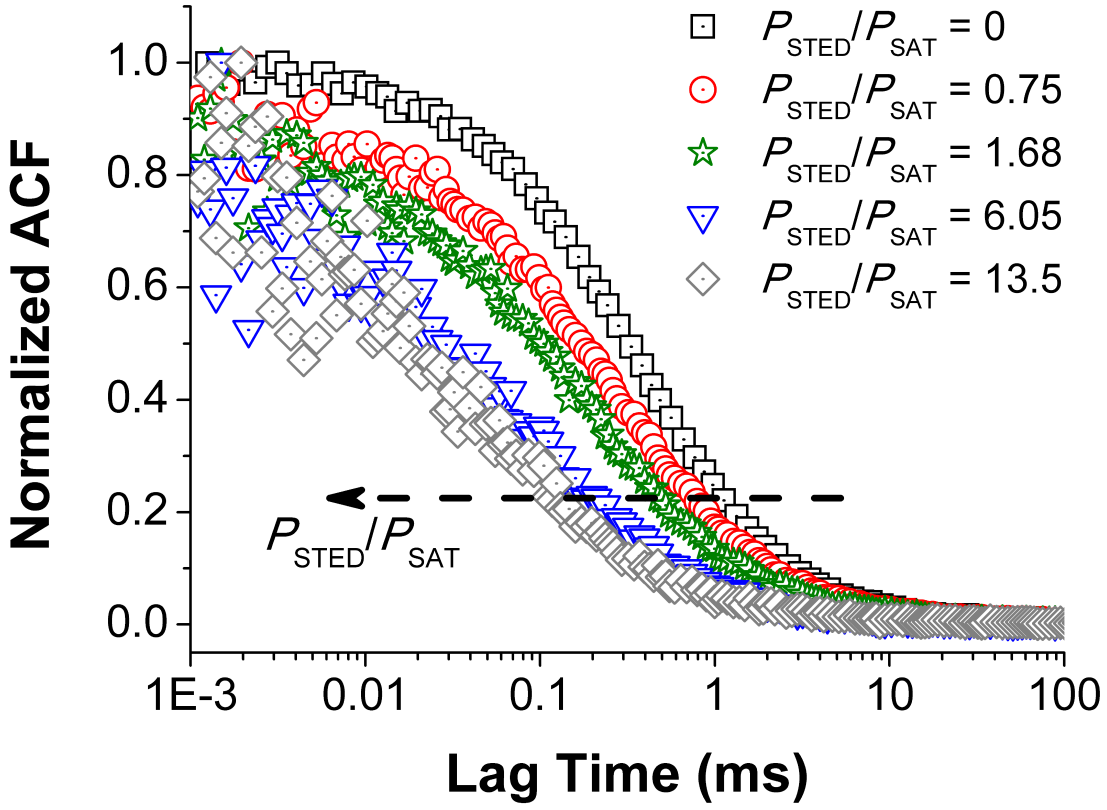

Figure S5: Experimental autocorrelation curves for ATTO647N in a $C_{12}E_8$ solution (293 μM) under various STED power settings.

We recorded the diffusion of ATTO647N in $C_{12}E_8$ solutions under various STED powers ($P_{\mathrm{STED}}/P_{\mathrm{SAT}} = 1 - 13.5$). The P_{SAT} of ATTO647N in phosphate-buffered saline (PBS), determined by finding the P_{STED} at which its fluorescence intensity dropped by half according to the definition of P_{SAT}, was equal to 11 mW. As expected, we clearly observed shifts of

autocorrelation curves towards the shorter lag time region with the increasing STED power (cf. Fig. S5). We were still able to collect smooth enough autocorrelation function curves at much higher STED power ($P_{\mathrm{STED}}/P_{\mathrm{SAT}} = 13.5$) in the micellar solutions compared to those in PBS ($P_{\mathrm{STED}}/P_{\mathrm{SAT}} = 1.7$). This could possibly be explained by the slower effective diffusion of the dyes in the micellar solutions, which increased the average number of photons per single passage of the probe through the observation volume and improved the photon statistics.

S7 Regimes of applicability of different autocorrelation models

STED-FCS allows to observe the transition from the effective diffusion of single-component (dyes) to the two-component diffusion (dyes and dye-micelle complexes) in a size-alterable volume and also quantitatively determine the equilibrium and rate constants of complex-formation using analytical models for the autocorrelation function. The regimes of applicability of different autocorrelation models are schematically depicted in Fig. S6.

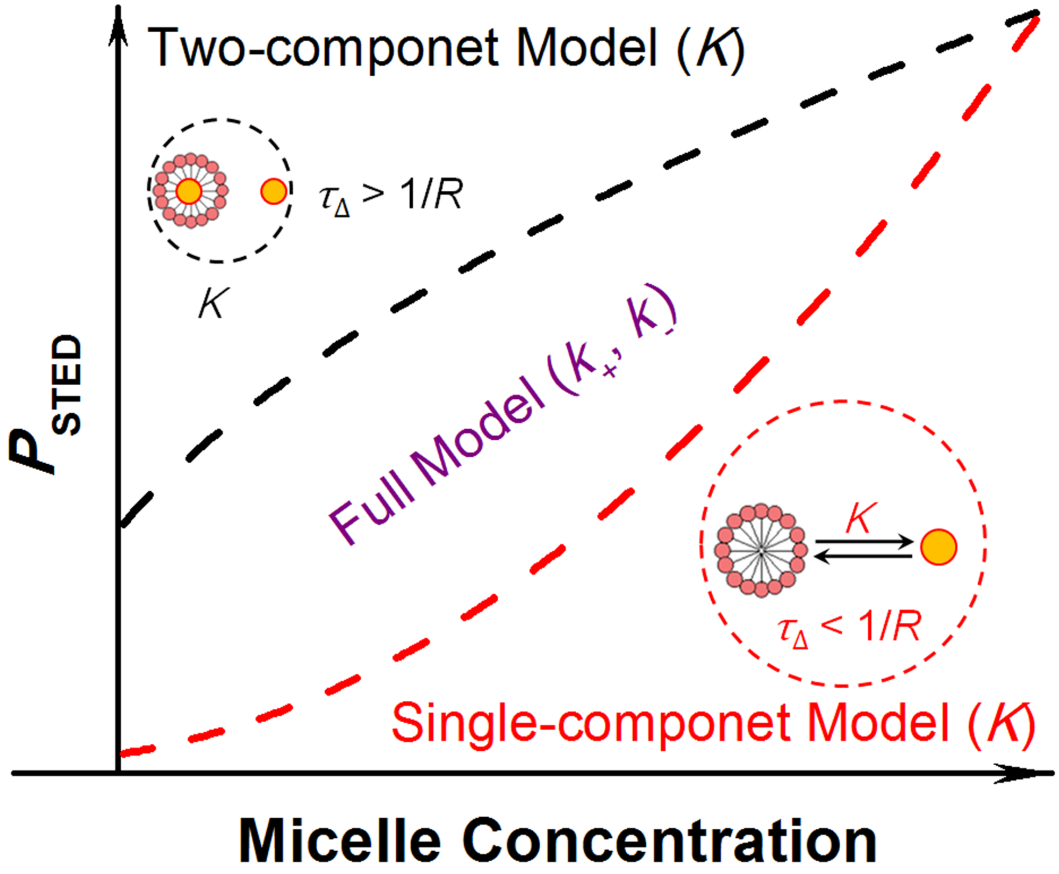

Figure S6: Illustration of the applicability of each model for the autocorrelation function in a diffusion-reaction system in STED-FCS. The single-component model (Eq. S2) is suitable for studies in the relatively concentrated solutions, while the two-component model (Eq. S3) is the limiting case, relevant to slow reaction and small observation volume. The equilibrium constant of the reaction can be determined in any of the cases. The full reaction-diffusion model (Eq. S1) can be applied to the systems falling between the two limiting cases (i.e. when $\tau_\Delta \approx 1/R$), allowing to retrieve information on the rate constants of complex formation.

References

(1) Schönau, T.; Siebert, T.; Härtel, R.; Eckhardt, T.; Klemme, D.; Lauritsen, K.; Erdmann, R. Pulsed picosecond 766 nm laser source operating between 1-80 MHz with automatic pump power management. *Proc. SPIE* **2013**, 860409.

(2) Clausen, M. P.; Sezgin, E.; de la Serna, J. B.; Waithe, D.; Lagerholm, B. C.; Eggeling, C. A straightforward approach for gated STED-FCS to investigate lipid membrane dynamics. *Methods* **2015**, *88*, 67–75.

(3) Vicidomini, G.; Moneron, G.; Han, K. Y.; Westphal, V.; Ta, H.; Reuss, M.; Engelhardt, J.; Eggeling, C.; Hell, S. W. Sharper low-power STED nanoscopy by time gating. *Nat. Methods* **2011**, *8*, 571–573.

(4) Moffitt, J. R.; Osseforth, C.; Michaelis, J. Time-gating improves the spatial resolution of STED microscopy. *Opt. Express* **2011**, *19*, 4242–4254.

(5) Zhang, X.; Poniewierski, A.; Jelińska, A.; Zagożdżon, A.; Wisniewska, A.; Hou, S.; Hołyst, R. Determination of equilibrium and rate constants for complex formation by fluorescence correlation spectroscopy supplemented by dynamic light scattering and Taylor dispersion analysis. *Soft Matter* **2016**, *12*, 8186–8194.

(6) Magde, D.; Elson, E. L.; Webb, W. W. Fluorescence correlation spectroscopy. II. An experimental realization. *Biopolymers* **1974**, *13*, 29–61.

(7) Hołyst, R.; Poniewierski, A.; Zhang, X. Analytical form of the autocorrelation function for the fluorescence correlation spectroscopy. *Soft Matter* **2017**, *13*, 1267–1275.

(8) Krichevsky, O.; Bonnet, G. Fluorescence correlation spectroscopy: the technique and its applications. *Rep. Prog. Phys.* **2002**, *65*, 251–297.

(9) Sozanski, K.; Sisamakis, E.; Zhang, X.; Holyst, R. Quantitative Fluorescence Corre-

lation Spectroscopy in 3D Systems under Stimulated Emission Depletion Conditions. *Optica* **2017**, *4*, 982–988.

(10) Dyba, M.; Keller, J.; Hell, S. Phase filter enhanced STED-4Pi fluorescence microscopy: theory and experiment. *New J. Phys.* **2005**, *7*, 134.

(11) Kapusta, P. Absolute diffusion coefficients: compilation of reference data for FCS calibration. 2010.